PCCP

PAPER

Theoretical ^{57}Fe Mössbauer spectroscopy: isomer shifts of [Fe]-hydrogenase intermediates†

Cite this: *Phys. Chem. Chem. Phys.*, 2014, **16**, 4853

Erik Donovan Hedegård,[a] Stefan Knecht,‡[a] Ulf Ryde,[b] Jacob Kongsted[a] and Trond Saue*[c]

Received 16th October 2013,
Accepted 14th January 2014

DOI: 10.1039/c3cp54393e

www.rsc.org/pccp

Mössbauer spectroscopy is an indispensable spectroscopic technique and analytical tool in iron coordination chemistry. The linear correlation between the electron density at the nucleus ("contact density") and experimental isomer shifts has been used to link calculated contact densities to experimental isomer shifts. Here we have investigated relativistic methods of systematically increasing sophistication, including the eXact 2-Component (X2C) Hamiltonian and a finite-nucleus model, for the calculation of isomer shifts of iron compounds. While being of similar accuracy as the full four-component treatment, X2C calculations are far more efficient. We find that effects of spin–orbit coupling can safely be neglected, leading to further speedup. Linear correlation plots using effective densities rather than contact densities *versus* experimental isomer shift lead to a correlation constant $a = -0.294\ a_0^{-3}$ mm s^{-1} (PBE functional) which is close to an experimentally derived value. Isomer shifts of similar quality can thus be obtained both with and without fitting, which is not the case if one pursues *a priori* a non-relativistic model approach. As an application for a biologically relevant system, we have studied three recently proposed [Fe]-hydrogenase intermediates. The structures of these intermediates were extracted from QM/MM calculations using large QM regions surrounded by the full enzyme and a solvation shell of water molecules. We show that a comparison between calculated and experimentally observed isomer shifts can be used to discriminate between different intermediates, whereas calculated atomic charges do not necessarily correlate with Mössbauer isomer shifts. Detailed analysis reveals that the difference in isomer shifts between two intermediates is due to an overlap effect.

1 Introduction

It is needless to emphasize the role of coordination compounds with an iron metal center in inorganic and bio-inorganic chemistry. Apart from the obvious industrial interest in iron coordination compounds, the biological role played by iron is unmatched by any other metal. For instance, enzymes comprising heme units have been found in essentially all lineages of life. Another example is hydrogenase enzymes[1,2] which are promising candidates for hydrogen storage materials.

An important spectroscopic technique in iron chemistry is Mössbauer spectroscopy.[3] Although also applicable to other nuclei, its use to characterize iron compounds is by far dominating.[4] Mössbauer spectroscopy relies on the Mössbauer effect, which is the recoilless emission or absorption of γ radiation from a nucleus in a (solid) sample. A common source to create excited-state iron nuclei is the radioactive ^{57}Co isotope, which decays by electron capture to the nuclear isomer ^{57m}Fe. The emitted γ-ray from the relaxation of the spin $I = 3/2$ to the nuclear ground $I = 1/2$ state of the iron nucleus is then used to probe the sample (absorber). The Mössbauer isomer shift effectively probes the electron density in the close vicinity of the nucleus, whereas the quadrupole splitting is sensitive to deviations from spherical symmetry. These two Mössbauer parameters therefore provide complementary information from which chemical descriptors such as the spin and the oxidation state of the Mössbauer-active atom can be extracted.[5]

In the present contribution we focus on the Mössbauer isomer shift. The electrostatic interaction between electronic and nuclear charge distributions,

$$E^{e0} = \int \rho_e(\mathbf{r}_e)\phi_n(\mathbf{r}_e;R)\mathrm{d}^3r_e; \quad \phi_n(\mathbf{r}_e;R) = \int \frac{\rho_n(\mathbf{r}_n;R)}{r_{en}}\mathrm{d}^3r_n \quad (1)$$

[a] *Department of Physics, Chemistry and Pharmacy, University of Southern Denmark, Campusvej 55, Odense 5420 M, Denmark. E-mail: edh@sdu.dk*
[b] *Department of Theoretical Chemistry, Lund University, Chemical Centre, P.O. Box 124, S-221 00 Lund, Sweden*
[c] *Laboratoire de Chimie et Physique Quantiques (UMR 5626), CNRS/Université Toulouse III – Paul Sabatier, 118 Route de Narbonne, F-31062 Toulouse cedex, France. E-mail: trond.saue@irsamc.ups-tlse.fr; Fax: +33 (0)561556031; Tel: +33 (0)561556065*

† Electronic supplementary information (ESI) available. See DOI: 10.1039/c3cp54393e

‡ Present address: Laboratory of Physical Chemistry, ETH Zürich, Wolfgang-Pauli-Straße 10, 8093 Zürich, Switzerland.

and notably its change upon nuclear excitation, may lead to a modification ΔE^{e0} of the nuclear γ-transition energy E_γ. The modification of the transition energy is in general different for the source (s) and the absorber (a) and gives rise to a non-zero isomer shift[6–8]

$$\delta = \frac{c}{E_\gamma}\left(\Delta E_a^{e0} - \Delta E_s^{e0}\right) \quad (2)$$

where c is the speed of light. The conversion factor of c/E_γ arises as the sample is brought to resonance by mechanically changing the relative motion of the source and sample, taking advantage of the Doppler effect. The isomer shift is accordingly given in units of speed, typically mm s^{-1}. In older literature, the Mössbauer isomer shifts were often reported with respect to the source material in which ^{57}Co was embedded, whereas today it is more common to use a well-defined reference, which thereby takes the place of the source in the above expression. Typical examples of Mössbauer references are iron foil (α-Fe) and sodium nitroprusside $Na_2[Fe(NO)(CN)_5]\cdot 2H_2O$.

The modulation of electrostatic interaction upon the change in nuclear size from ground to excited nuclear state can be expressed in terms of a first-order Taylor expansion.[9–12] Neglecting any dependence of the electronic density ρ_e on nuclear radial size then leads to

$$\Delta E^{e0} = \left.\frac{\partial E^{e0}}{\partial R}\right|_{R=R_0} \Delta R \approx \int \rho_e(\mathbf{r}_e) \left.\frac{\partial \phi_n(\mathbf{r}_e; R)}{\partial R}\right|_{R=R_0} \mathrm{d}^3 r_e \, \Delta R \quad (3)$$

where ΔR is change in the radial size parameter R between the excited and the ground nuclear state. Since the derivative of the nuclear potential ϕ_n is an extremely local quantity one may formally extract an effective density $\bar{\rho}_e$, that is, the weighted average of the electron density over the finite-sized nucleus, from the integral:

$$\Delta E^{e0} = \bar{\rho}_e \int \left.\frac{\partial \phi_n(\mathbf{r}; R)}{\partial R}\right|_{R=R_0} \mathrm{d}^3 r \, \Delta R \quad (4)$$

This leads to the following expression for the Mössbauer isomer shift

$$\delta = \alpha(\bar{\rho}_e - \bar{\rho}_e^{\mathrm{ref}}), \quad (5)$$

where the isomer shift calibration constant

$$\alpha = \left(\frac{4\pi Z c R_0^2}{5E_\gamma}\right)\frac{\Delta R_0}{R_0} \quad (6)$$

contains all constants and nuclear information. The effective density $\bar{\rho}_e$ is usually approximated by the contact density ρ_0, that is, the electron density at the nuclear origin. By convention, these are taken to be positive quantities, representing the number rather than charge density of electrons. For heavier nuclei the use of contact rather than effective densities has been shown to give sizeable errors,[13,14] on the order of 10%, but which can be corrected for due to their systematic nature. However, there is no computational gain in using contact densities rather than effective densities.[14]

Most quantum chemical calculations of the Mössbauer isomer shift exploit the linear correlation

$$\delta = a(\bar{\rho}_e - C) + b. \quad (7)$$

between the experimental isomer shift and the effective density, the latter usually approximated by the contact density.[15–18] This *ansatz* allows us to absorb not only nuclear information, but also shortcomings of the chosen theoretical model chemistry into the fitting constants a and b (C is held constant in the fit), and so a is in general not equal to the calibration constant α. The first computational studies to make use of fitting expressions such as eqn (7) were based on relativistic but rather crude semi-empirical or Hartree–Fock methods.[15–17,19] Later, modern density functional theory with gradient corrected functionals were applied with success,[20–22] but without taking into account relativistic effects at all. Such an *ansatz* relies on error cancellations[18] and suffers from the fact that each new combination of the functional (method) and basis set gives a new correlation line (eqn (7)). The fitting scheme is efficient and fairly reliable, though. In a recent calibration study Bochevarov *et al.* found errors in the range 0.02–0.04 mm s^{-1} for a carefully chosen test set and suggested errors on the order of 0.1 mm s^{-1} for calculations on more complex systems.[23]

Filatov and co-workers have suggested a method that they claim to be independent of fitting.[9,24,25] As demonstrated below, this is almost true. In this model the isomer shift is calculated directly from eqn (5) using an internal reference and a value of the isomer shift calibration constant $\alpha = -0.31 \pm 0.04$ a_0^3 mm s^{-1} extracted from experiment. This value may be compared to the consensus value $\alpha = -0.267 \pm 0.115$ a_0^3 mm s^{-1} proposed by Oldfield and co-workers[20] based on computational calibration studies, as well as the more recent value $\alpha = -0.291$ a_0^3 mm s^{-1} obtained by Wdowik and Ruebenbauer in a series of relativistic solid-state DFT + U calculations using the PBE functional.[26] The α value recommended by Kurian and Filatov was obtained by Ladrière *et al.*[27] by combining experimental ^{57}Fe isomer shifts with differential measurements of the electron capture rate $\lambda_{EC} = (\ln 2) t_{EC}^{-1}$ of ^{52}Fe in different iron compounds, both being proportional to the contact density. The final value was then obtained by in addition using the measured[28] half-life t_{EC} of ^{52}Fe as well as the contact density $\rho_0 = 15\,070$ a_0^{-3} extracted from numerical 4-component relativistic Hartree–Fock calculations[29] on $Fe^{2+}(d^6)$. The quoted value is accordingly not purely experimental, but depends on a single calculated contact density. However, the absolute value of the contact density is by far less sensitive than relative values to different chemical environments and computational models, considering that an isomer shift of 1 mm s^{-1} corresponds to a change of ~200 ppm of the contact density. On the other hand, beyond experimental errors in the electron capture rate there are also uncertainties in the theoretical foundations related to the proper inclusion of the electronic wave function leading to so-called overlap and exchange effects.[30] We have nevertheless in the present contribution chosen to explore the scheme proposed by Filatov and co-workers using the quoted value of α, taking *molecular* $[Fe(NO)(CN)_5]^{2-}$ as internal reference and, unless otherwise stated, using the *effective* densities $\bar{\rho}_e$ rather than contact densities ρ_0.

The most rigorous relativistic *ansatz* presented in this work is based on the Dirac–Coulomb (DC) Hamiltonian

$$\hat{H} = \sum_i \left\{c(\boldsymbol{\alpha}\cdot\boldsymbol{p}_i) + \beta' mc^2 + V_{eN}\right\} + \sum_{i<j}\frac{1}{r_{ij}} + V_{NN} \quad (8)$$

where $\beta' = \beta - I$ and $\boldsymbol{\alpha}$ and β are the 4×4 Dirac matrices

$$\beta = \begin{pmatrix} I & 0 \\ 0 & -I \end{pmatrix} \qquad \boldsymbol{\alpha} = \begin{pmatrix} 0 & \boldsymbol{\sigma} \\ \boldsymbol{\sigma} & 0 \end{pmatrix}, \tag{9}$$

I is the identity matrix and $\boldsymbol{\sigma}$ are the Pauli spin matrices. The DC Hamiltonian includes electron–electron repulsion through the instantaneous Coulomb interaction. This corresponds to the zeroth-order term of an expansion of the full relativistic two-electron interaction in orders of c^{-2}, which is sufficient for most chemical purposes.[31] Although the two-electron operator in the Dirac–Coulomb Hamiltonian has the same form as the non-relativistic electronic Hamiltonian, its physical content is different, for instance giving rise to spin-same orbit interaction.[32]

There are several ways to transform the Hamiltonian in eqn (8) into a two-component Hamiltonian, thereby reducing the complexity of the computational problem.[32] One such Hamiltonian is based on the Zeroth Order Regular Approximation[33,34] (ZORA) and has been used extensively in Mössbauer studies. Filatov and coworkers[9,11,24,25,35] have introduced the use of the Normalized Elimination of the Small Component (NESC).[36] In the present work we investigate the performance of the closely related eXact 2-Component (X2C) Hamiltonian – with and without spin–orbit coupling – using the formalism of ref. 37. To the best of our knowledge, this is the first presentation of four-component DFT and two-component CCSD(T) calculations of Mössbauer isomer shifts on larger inorganic molecules. Since two-component methods at the SCF level are by far computationally less costly than four-component methods they will significantly broaden their applicability provided that similar accuracy can be reached within both approaches. All relativistic methods are compared to the non-relativistic Hamiltonian where both a finite sized and a point charge nuclei were employed. As a test set for the various relativistic models, we consider the closed-shell molecules **1–5**, displayed in Fig. 1.

A second objective of this study is to investigate the use of a relativistic computational protocol in bio-inorganic chemistry and what advantages are possibly accrued by such an approach. To this end, we selected the recently characterized [Fe]-hydrogenase[38–40] which stands out from other classes of hydrogenases as it contains no iron–sulfur clusters as well as only a mono-nuclear metal site. Mössbauer studies on [Fe]-hydrogenase have been carried out by Shima and co-workers.[41] In this paper we use the correlation plots from molecules **1–5** to calculate isomer shifts for the [Fe]-hydrogenase intermediates. These isomer shifts are then compared to the experimental data. It is noted that molecules **1–5** are well suited for this purpose, having the same spin states and similar ligands as the [Fe]-hydrogenase active site. To investigate whether the X2C *ansatz* is more generally applicable for iron compounds, we will in a follow-up study extend the admittedly limited set **1–5** to comprise also open-shell iron complexes.

Despite having a somewhat simpler structure than the bi-metallic hydrogenase enzymes, the reaction mechanism of the H_2 splitting in [Fe]-hydrogenase is not yet known. Structure **6** (Fig. 1) is a model of the structurally characterized enzyme, while **7** and **8** are models of two intermediates, which were recently proposed to be involved in the mechanism of H_2 cleavage.[42] We have computed the isomer shift of all three molecules, **6–8**, where the respective geometries have been optimized by a QM/MM procedure including the full protein, surrounded by a water sphere of 60 Å from the protein center.

Very recently, after the submission of the first version of the present work, Gubler *et al.*[43] reported a detailed computational study of [Fe]-hydrogenase intermediates based on the relativistic high-order Douglas–Kroll–Hess Hamiltonian. Compared to the present work, the study features a larger reference set of iron compounds for calibration, provides both isomer shifts and quadrupole splittings and also considers a larger variety of coordinations around iron. On the other hand, the [Fe] hydrogenase models have been optimized at the DFT level using a Continuum Solvation Model (COSMO) and so do not take into account the protein environment as in the present study. Furthermore, as will be seen in the following, the present study contains a more detailed analysis of variations in the isomer shifts between the [Fe] hydrogenase model structures.

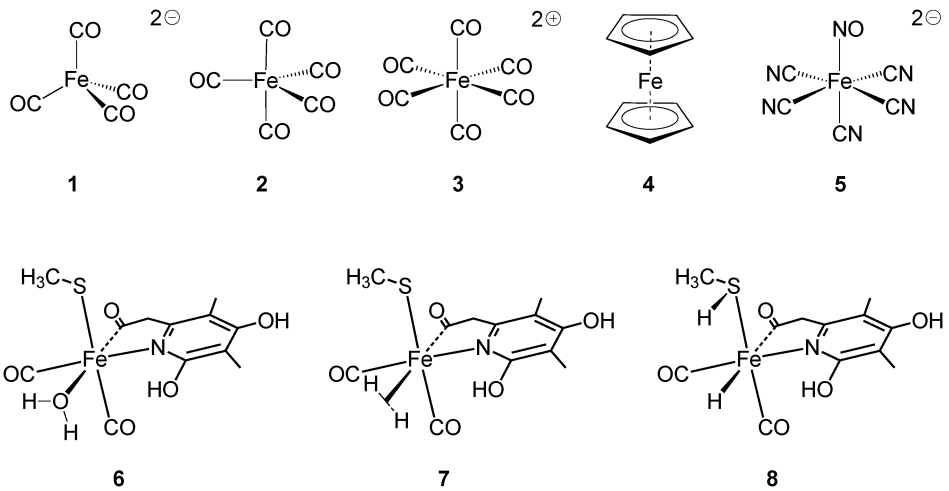

Fig. 1 Structures used in this study. Molecules **1–5** are used for investigating the relativistic methods, while **6–8** are the target model structures of [Fe]-hydrogenase.

The paper is organized as follows: in Section 2 we specify our computational protocol. Next, in Section 3.1, we present a calibration study of ^{57}Fe isomer shifts obtained at various levels of theory and with comparison to experiment. Then, in Section 3.2, we apply our final best model to the isomer shift determination of [Fe]-hydrogenase model systems and provide a detailed analysis of what factors modulate the isomer shift between the different structures. Finally, in Section 4, we draw conclusions and give an outlook to ongoing future work.

2 Computational details

The applied test set comprises the molecules **1–5** displayed in Fig. 1. The structures of **1–5** were optimized with the Gaussian09 program[44] using the BP86 functional[45,46] and a TZVP basis set for all atoms.[47,48] The experimental isomer shifts used as reference data in this study are provided in Table S1 in the ESI.† The models of the [Fe]-hydrogenase intermediates **6–8** (see Fig. 1) have been optimized with DFT, considering the immediate coordination geometry of iron as the QM region and including a full protein matrix. The optimization was performed using the QM/MM procedure defined by the ComQum program.[49,50] From the fully optimized structures the active site model was cut out as shown in Fig. 1. Further details concerning these optimizations will be published elsewhere.

All relativistic calculations were carried out with a development version of the DIRAC program package.[51] For molecules **1–5**, calculations were performed with the Dirac–Coulomb Hamiltonian including all integral classes arising from the two-electron Coulomb term (keyword .DOSSSS). The next level of approximation was to use an eXact 2-component Hamiltonian,[37] both spinfree and with spin–orbit coupling, where in the latter case two-electron spin-same orbit corrections were obtained by an atomic mean-field integral (AMFI) approximation.[52,53] In the case of the [Fe]-hydrogenase intermediates **6–8** the X2C Hamiltonian was exclusively applied.

SCF calculations for the molecules **1–5** were performed at the Hartree–Fock and the DFT level of theory, respectively. For the latter, several exchange–correlation functionals were chosen, namely LDA (VWN5)[54] (results shown in the ESI†), PBE[55] and PBE0.[56] The [Fe]-hydrogenase intermediates **6–8** were studied with PBE0 only. A Dunning cc-pVTZ basis set[57] was employed for all ligand atoms, while for iron we used a triple-ζ Dyall basis set[58] augmented with one steep s-function (ξ_s = 3.02252694 × 10^8) and one steep p function (ξ_p = 1.83449497 × 10^5). All basis sets were kept in their uncontracted form for the SCF calculations, which is necessary in the current implementation of the AMFI approximation. To facilitate a direct comparison between Hamiltonians basis sets were kept uncontracted also in the spinfree X2C and non-relativistic Hamiltonian framework. Spinfree X2C Coupled-Cluster (CC) calculations with contracted ligand atom basis sets[59] have been performed for the molecules **1–3** and **5**. The ferrocene complex (**4**) is computationally quite demanding and has not been considered at the CC level. Following the standard protocol in experimental studies, we refer to **5** as a reference in the CC calculations. The calculations were carried out with the Relativistic Coupled Cluster (RELCCSD) module of DIRAC.[60–62] Contact densities were calculated based on the prescription by Knecht *et al.*[14] for mercury compounds. Accordingly, the correlation contribution $\rho_0^{\text{corr.}}$ is derived from finite-field calculations which is added to the analytical HF value, ρ_0^{HF}. Details are given in the ESI.† We refer to ρ_0^{MP2}, ρ_0^{CCSD} and $\rho_0^{\text{CCSD(T)}}$ to denote the sum of ρ_0^{HF} and $\rho_0^{\text{corr.}}$ for a given correlated method. A careful investigation revealed that a 5-point stencil in combination with an optimal field strength of $h = 10^{-7}$ a.u. is required to obtain reliable MP2 and CC contact densities from the finite-differentiation approach. The occupied active space in the CC calculations was chosen to comprise in each case the $(n-1)$sp $n$sp shell of the ligand atoms (outer core and valence shells) as well as the $(n-1)$spd ns shell of iron. A high cutoff in the active virtual space at $\approx 15-16\ E_h$ ensured that all important core-valence and valence correlating functions were taken into account. All remaining occupied core orbitals as well as virtual orbitals were kept frozen.

For the projection analysis[63,64] we calculated the atoms in their electronic ground state configuration using fractional occupation and employed all occupied orbitals of the atoms, adding a second s orbital of the hydrogens as well as the 4p orbitals of iron. This set of atomic orbitals does not span the molecular orbitals fully: the polarization contribution amounts to about one electron, which is slightly high, but constant for all three molecules and has negligible contribution to the contact and effective densities. We are therefore confident that the projection analysis is reliable for systems **6–8**.

3 Results and discussion

3.1 Calibration study

In this section we first compare three different relativistic Hamiltonians of increasing accuracy. We also comment on the use of CC data in iron Mössbauer spectroscopy, and relate the data obtained here to previous benchmark studies. Next, a method which employs fitting, eqn (7), and a method that does not require fitting, eqn (5), are compared to experiment with respect to their performance. The results from this calibration study are then used to investigate [Fe]-hydrogenase intermediates as displayed in Fig. 1.

3.1.1 Comparison of relativistic models and methods. Calculated effective densities *versus* the experimental Mössbauer shifts are shown in Fig. 2 for the relativistic (top) and non-relativistic Hamiltonians (bottom). Both classes of Hamiltonians show a good linear correlation, as could be expected. The fitting constants have been compiled in Tables 1 and 2 for the PBE and PBE0 functionals, respectively. All the experimental data used for the fitting have been compiled in Table S1 in the ESI† and are given relative to iron foil (α-Fe). Starting with the relativistic methods in Fig. 2 (top), there are clear differences in the absolute effective densities obtained with the different relativistic Hamiltonians. The trends, however, are identical,

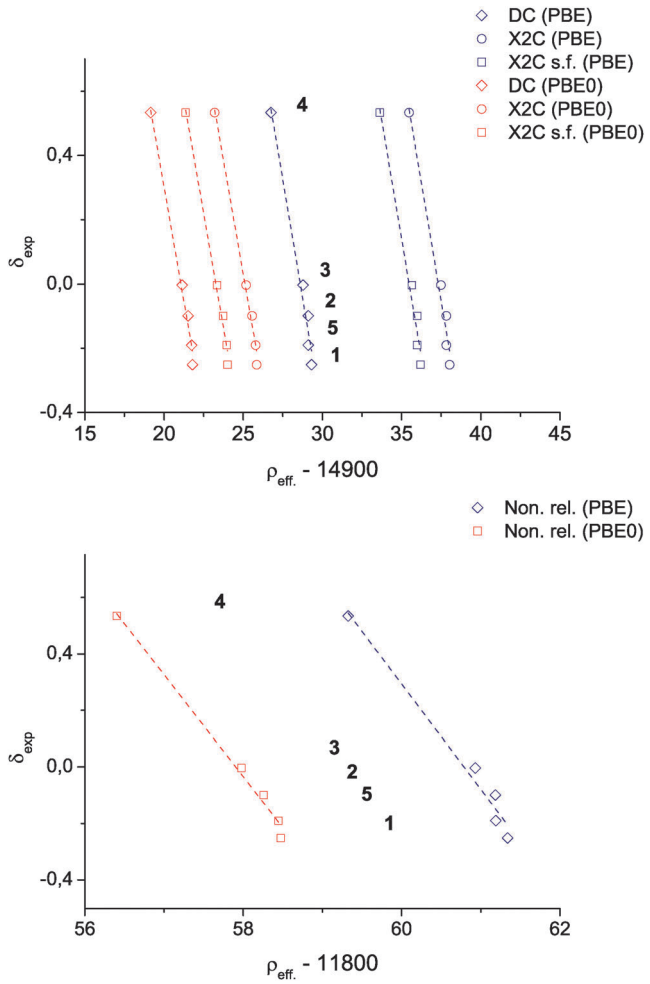

Fig. 2 Correlation between effective densities (in a_0^{-3}) on iron and experimental isomer shifts (eqn (7); in mm s^{-1}). DC is the Dirac–Coulomb Hamiltonian, X2C is the eXact two-Component Hamiltonian and X2C (s.f.) refers to the X2C spin-free variety.

which is also reflected in the slopes of the linear correlation plots. In fact, the change between the PBE0 hybrid functional and the PBE GGA functional is larger than the change within the relativistic level of approximation. A comparison between the X2C and its spin-free version reveals that spin–orbit effects are rather small for the iron compounds studied here even though we are concerned with a property near the heavy iron nucleus. Taking into account scalar relativistic effects is on the other hand mandatory as can be seen from the large difference in both *a* and *b* parameters between the spin-free X2C Hamiltonian and the non-relativistic calculations. Though the data are not shown here, contact densities were also calculated using both the PBE and PBE0 functionals and all relativistic Hamiltonians (parts of these data are provided in the ESI†). The contact densities are generally, as expected, slightly larger in absolute numbers than the effective densities, but give rise to very similar isomer shifts. Thus the effect of using contact rather than effective densities is small. From comparing contact densities between non-relativistic calculations with and without finite nucleus models, the effect of the finite nucleus treatment is found to be negligible. However, it should be stressed that a finite nucleus treatment becomes mandatory in four- or two-component relativistic calculations due to the weak singularity in the relativistic wave function at the origin of a point nucleus.

In order to have high-quality computational reference data, Coupled Cluster (CC) calculations were performed. As a by-product, it allowed us to investigate the effect of taking into account an increasing level of electron correlation, by comparing with Hartree–Fock (HF), second-order Møller–Plesset (MP2) and Coupled Cluster with Single and Doubles (CCSD). A subset of the CC results is listed in Table 3, while the complete set has been compiled in the ESI.† An inspection of Table 3 reveals that the trends in HF and the DFT functionals are similar (and correlate linearly with the experimental trend). Inclusion of dynamical correlation through MP2 leads to isomer shifts which are significantly off. CCSD is again closer to the trend observed for HF, DFT and experiment, but $Fe(CO)_5$ is still an outlier. Perturbative inclusion of triples was also attempted, but did not yield a particular improvement. In fact, while the change for ρ_0^{CCSD} to $\rho_0^{CCSD(T)}$ in molecules **1–3** was rather moderate, the change for $[Fe(NO)(CN)_5]^{2-}$ (**5**) was surprisingly high (see Table S4 in the ESI†), leading to very large shifts (since **5** was used as reference). The trends for CCSD(T)

Table 1 Fitting parameters (eqn (7)) for the correlation plots in Fig. 2 with the PBE functional. In all cases *C* is kept fixed under the fit. Uncertainties are shown in parentheses. R^2 refers to the adjusted coefficient of determination

Method	DC	X2C	X2C (s.f.)	Non-rel
a (mm s^{-1} a_0^{-3})	−0.294 (0.02)	−0.294 (0.02)	−0.294 (0.02)	−0.373 (0.03)
b (mm s^{-1})	8.413 (0.711)	10.970 (0.926)	10.444 (0.881)	22.644 (1.968)
C (a_0^{-3})	14 900	14 900	14 900	11 800
R^2	0.9721	0.9721	0.9721	0.9705

Table 2 Fitting parameters (eqn (7)) for the correlation plots in Fig. 2 with the PBE0 functional. In all cases *C* is kept fixed under the fit. Uncertainties are shown in parentheses. R^2 refers to the adjusted coefficient of determination

Method	DC	X2C	X2C (s.f.)	Non-rel
a (mm s^{-1} a_0^{-3})	−0.284 (0.02)	−0.284 (0.02)	−0.284 (0.01)	−0.360 (0.021)
b (mm s^{-1})	5.975 (0.304)	7.121 (0.393)	6.612 (0.336)	20.873 (1.233)
C (a_0^{-3})	14 900	14 900	14 900	11 800
R^2	0.9897	0.9897	0.9898	0.9881

Table 3 Relative contact densities ($\Delta\rho_0$) calculated with various methods. The $\Delta\rho_0$ values are reported wrt. $[Fe(NO)(CN)_5]^{2-}$ and are given in a_0^{-3}. All results are calculated with the spin-free X2C Hamiltonian

Method	$\Delta\rho_0^{HF}$	$\Delta\rho_0^{MP2}$	$\Delta\rho_0^{CCSD}$	$\Delta\rho_0^{PBE}$	$\Delta\rho_0^{PBE0}$
$[Fe(CO)_4]^{2-}$	0.60	−1.87	0.05	0.21	0.06
$Fe(CO)_5$	−0.37	0.35	0.65	0.00	−0.23
$[Fe(CO)_6]^{2+}$	−1.13	−0.82	−0.69	−0.33	−0.61

and CCSD are, however, similar. Thus, with the exclusion of $Fe(CO)_5$, PBE0 and CCSD provide very similar shifts in contact density, but both the small size of the test set and the spurious large change in contact density upon inclusion of the (perturbative) triples correction for $[Fe(NO)(CN)_5]^{2-}$ render the current conclusion very tentative with respect to a comparison of the CC and DFT results. The fact that perturbative treatments are seen to be problematic, along with rather high T_1 amplitudes, indicates large orbital relaxation effects and/or a potential multiconfigurational ground state wave function, as has previously been observed for iron nitrosyl complexes (see ref. 65–67 and references therein). A similar conclusion for $Fe(CO)_5$ was reached by Schwerdtfeger *et al.*[68] in relation to estimation of the nuclear quadrupole moment of the excited $I = 3/2$ nuclear state of ^{57}Fe. Thus, it is likely that at least a full inclusion of triples and possibly quadruples or a inherently multiconfigurational treatment, for example CASSCF followed by multireference CC or CI, is necessary to obtain reliable high-quality results. The former is possible in the DIRAC code through the interface[69] to the MRCC program of M. Kállay,[70,71] but demands at present computational resources beyond our capabilities. Some of the molecules from our test set have also been used by others to validate computed isomer shifts. For the molecules **2** and **4** the different molecular geometries used hamper a direct comparison with the studies reported by Kurian and Filatov.[24,25] Furthermore, the results are often reported in a different manner, either in total densities or in isomer shifts with respect to a reference (eqn (5) with α from ref. 24). After correcting for the reference compounds, the relative values between $[Fe(CO)_4]^{2-}$ and $Fe(CO)_5$ are in reasonable agreement. In addition, we find an acceptable agreement of the total density of $Fe(Cp)_2$ obtained by us compared to the value reported in ref. 25. Using the double hybrid functional B2PLYP Kurian and Filatov arrive at a correlation constant of $a = -0.306\ a_0^{-3}$ mm s^{-1} which compares quite well with our value from the fully relativistic calculations in Tables 1 and 2.

The fitting constants obtained in the present work may be compared to those obtained by Gubler *et al.*[43] Using the 20th order spin-free DKH Hamiltonian, the B3LYP functional and 15 reference molecules they report a slope $a = -0.263$ mm s^{-1} a_0^{-3}, whereas reduction of the reference set to 10 molecules with isomer shifts in the range ± 0.1 mm s^{-1} changes the slope to $a = -0.285$ mm s^{-1} a_0^{-3}, tantalizingly close to our value obtained with the PBE0 functional and the spin-free X2C Hamiltonian (*cf.* Table 2).

3.1.2 Comparison to experiment. In Table 4 the calculated isomer shifts are compared to experiment, by using either eqn (7) and the appropriate fitting constants (Tables 1 and 2) or eqn (5) with $[Fe(NO)(CN)_5]^{2-}$ as reference.

In the case of fitting, good results can be obtained both with and without relativistic effects. This is mainly caused by the large difference in linear correlation constants, a, between non-relativistic and relativistic methods. Thus, the non-relativistic methods are indirectly corrected through a. Since the linear correlation constant a is rather close to the experimentally derived α[27] within all relativistic methods, the best result is indeed obtained with an inclusion of relativistic effects even for a first-row transition metal such as iron.

In conclusion, both relativistic and non-relativistic methods can be used to estimate shifts for iron Mössbauer spectroscopy. However, the most coherent and transparent results are obtained using relativistic methods, leading to similar results for approaches which employ fitting procedures and those based on the use of a reference compound.

A note concerning $Fe(CO)_5$ should be made. For this compound Zhang *et al.*[20] reports an isomer shift of −0.18 mm s^{-1}, a value subsequently adopted by Nemykin and Hadt.[72] Zhang *et al.* cite an experimental paper by Kerler and co-workers[73] which gives

Table 4 Calculated and experimental isomer shifts (mm s^{-1}) for molecules **1–5**. The calculation of isomer shifts is performed with the Dirac–Coulomb (DC), eXact two-Component (X2C) or the spin-free X2C Hamiltonians, using either eqn (7) or (5). The different experimental values are due to difference in reference compounds. Values are given for the PBE0 functional with PBE in parentheses

	$[Fe(CO)_4]^{2-}$	$Fe(CO)_5$	$[Fe(CO)_6]^{2+}$	$Fe(Cp)_2$	$[Fe(NO)(CN)_5]^{2-}$
Fit[a]					
DC	−0.209 (−0.209)	−0.128 (−0.147)	−0.020 (−0.048)	0.542 (0.544)	−0.192 (−0.148)
X2C	−0.209 (−0.209)	−0.128 (−0.147)	−0.020 (−0.048)	0.542 (0.544)	−0.192 (−0.148)
2C (s.f.)	−0.209 (−0.209)	−0.128 (−0.147)	−0.020 (−0.048)	0.542 (0.544)	−0.192 (−0.148)
Non-rel	−0.205 (−0.205)	−0.127 (−0.147)	−0.023 (−0.051)	0.543 (0.545)	−0.194 (−0.149)
Exp.	−0.251	−0.09	−0.003	0.534	−0.191 (3)
No fit[b]					
DC	−0.018 (−0.064)	0.071 (0.000)	0.189 (0.103)	0.813 (0.729)	0.000 (0.000)
X2C	−0.018 (−0.064)	0.071 (0.000)	0.189 (0.103)	0.813 (0.730)	0.000 (0.000)
X2C (s.f.)	−0.018 (−0.064)	0.071 (0.000)	0.189 (0.103)	0.812 (0.729)	0.000 (0.000)
Non-rel	−0.009 (−0.046)	0.058 (0.002)	0.146 (0.080)	0.634 (0.578)	0.000 (0.000)
Exp.	−0.061	0.10	0.187	0.724 (0.000)	0.000 (0.000)

[a] The isomer shift is calculated with eqn (7) using the parameters from Table 2. The experimental values refer to iron foil (α-Fe). [b] The isomer shift is calculated from eqn (5) with $\alpha = -0.31\ a_0^3$ mm s^{-1} using $[Fe(NO)(CN)5]^{2-}$ as reference.

isomer shifts of $Fe(CO)_5$ in both solid state, in frozen matrix and in solution and at different temperatures. The solid state value at the lowest reported temperature (143 K) is -0.447 mm s^{-1} relative to ^{57}Co in platinum at room temperature.[74] Converting to α-iron at 300 K using +0.3484(24) mm s^{-1} taken from ref. 4 we obtain an isomer shift of -0.099 mm s^{-1} which we have employed in the present work. Curiously Zhang *et al.* cite the same experimental paper for their value of -0.18 mm s^{-1}, as do Kurian and Filatov[25] who report -0.140 mm s^{-1}. More recent experimental isomer shifts for $Fe(CO)_5$ are reported by Greatrex and Greenwood[75] and Kuhn *et al.*[76] who report +0.17 mm s^{-1} (77 K) and +0.18 mm s^{-1} (113 K), respectively, both using hydrated sodium nitroprusside at room temperature as reference, which translates into -0.088 mm s^{-1} and -0.078 mm s^{-1} relative to α-Fe foil. Finally, for completeness, a Mössbauer isomer shift of -0.174 mm s^{-1} is reported by De Paoli *et al.*[77] at 4.2 K for $Fe(CO)_5$ sorbed in a polymer film. The reference appears to be ^{57}Co in rhodium, which converts to -0.05 mm s^{-1} relative to α-iron.

We conclude this subsection by commenting on the performance of the different DFT exchange–correlation functionals. This issue has been widely discussed for isomer shifts and it seems to be a common conclusion that functionals with a high amount of exact exchange are to be preferred.[10,23,24] Yet, using the X2C Hamiltonian and for the molecules investigated here, we find that the PBE functional performs well and is not inferior to the hybrid version PBE0 – the latter having a high amount of exact exchange (25%).

3.2 Hydrogenase intermediates

3.2.1 Isomer shifts. Encouraged by the results from the previous subsection, we have applied the X2C/DFT model to a biologically relevant iron system, namely the [Fe]-hydrogenase active site. The [Fe]-hydrogenase protein is found in certain methanogenic archaea and catalyzes the oxidation of H_2 in an intermediate step of the reduction of CO_2 to methane. H_2 is presumably split by coordination to iron and a hydride abstracted by N^5,N^{10}-methenyl-tetrahydromethanopterin (methenyl-H_4MPT^+), but the detailed mechanism is still under debate.[40,78,79] A crystal structure of [Fe]-hydrogenase was reported by Shima *et al.*,[39] but the iron ligation was later reinterpreted following a X-ray crystallographic study of a mutated protein.[38] Shima and co-workers also carried out a Mössbauer study of the full protein finding that the isomer shift did not change upon addition of H_2.[41] In the proposed catalytic mechanism, hydrogen activation is initiated by the H_2O/H_2 exchange in **6** to form **7** (see Fig. 1). In a computational study[42] Yang and Hall found that the free energy barrier of H_2 cleavage in **7** to form the thermodynamically more stable **8** (-3.4 kcal mol^{-1}) was quite low (6.6 kcal mol^{-1}) and therefore suggested **8** as the resting state observed in the Mössbauer experiment. They further argued that the isomer shifts of **7** and **8** would be quite similar since the Mulliken charges of iron in the two species are quite close (+0.142 and +0.138). We have, however, calculated the isomer shifts of all three species, as shown in Table 5. As can be seen from our results the isomer shift of **8** is appreciably different from the predicted isomer shift of **6** and **7**. An indirect estimate of Mössbauer isomer shifts based on Mulliken charges can accordingly not be recommended. The isomer shifts of **6** and **7** are on the other hand quite close to the experimental value, in particular when taking into account that the typical experimental error is ±0.01 mm s^{-1}.[41] Hence, according to our present results it seems likely that an intermediate of the type **7** would go unnoticed in a Mössbauer study. On the other hand, the hydride intermediate **8** has a calculated isomer shift which is significant off the experimental shift, and quite different from both **6** and **7**. This observation leads us to conclude that **8** does not build up in significant concentrations during the Mössbauer experiment, although **8** could still be involved in the catalytic cycle. In addition, it should be emphasized that the current studies are performed without taking into account the (methenyl-H_4MPT^+) substrate, which, according to ref. 41, is supposed to have only a minor effect on the isomer shift (suggesting rather small changes in the iron coordination sphere). To shed further light on the latter issue we are pursuing at present QM/MM optimizations of **6–8** that include the substrate.

Table 5 Isomer shifts (mm s^{-1}) calculated for molecules **6–8** with the X2C Hamiltonian and the PBE0 functional, using either eqn (7) or (5). A single experimental value is given since the Mössbauer isomer shift did not change upon addition of H_2.[41] Note that for the intermediate **8**, the $^{\ominus}$SCH3 group is altered to a protonated HSCH3 group (see Fig. 1)

$[Fe(L)(pyridone)(CO)_2(SCH_3)]^+$	L = H_2O (**6**)	L = H_2 (**7**)	L = $H^{\ominus}$ (**8**)	Exp.
Isomer shift[a]	0.059	0.049	−0.088	0.060
Isomer shift[b]	0.275	0.264	0.114	0.250

[a] The isomer shift is calculated from eqn (7) using the parameters from 1. The experimental values refer to iron foil (α-Fe). [b] The isomer shift is calculated from eqn (5) with $\alpha = -0.31$ using $[Fe(NO)(CN)_5]^{2-}$ as reference.

Gubler *et al.*[43] report isomer shifts 0.03, 0.02 and -0.02 mm s^{-1}, respectively, for their model structures corresponding to **6–8** and conclude, as we do, that the hydride species **8** is not the resting state of [Fe]-hydrogenase, contrary to the proposal of Yang and Hall.[42] As seen from Table 5, these values are somewhat different from ours, but can be converted to 0.07, 0.06 and 0.02 mm s^{-1} using their fitting parameters obtained by restricting the reference set to those having isomer shifts in the range ±0.1 mm s^{-1}. Again comparing with Table 5, the shifts for structures **6** and **7** match our results as well as experiment quite well, whereas a significant discrepancy remains for structure **8**. The latter feature certainly arises from our different computational protocols, with perhaps our inclusion of the full protein environment in the geometry optimizations as a decisive difference.

3.2.2 Projection analysis. The difference of 0.137 mm s^{-1} in calculated isomer shifts of molecules **7** and **8** shown in Table 5 translates into around 40–41 ppm change of contact density. Gubler *et al.*[43] attributes the difference to the fact that the negative charged hydride is a strong donor. However, from such a mechanism one would expect that the atomic charge of iron in **7** and **8** would be appreciably different, which is in contradiction with the Mulliken charges reported by Yang and Hall[42] as well as the atomic charges we report below. In fact, the underlying mechanism is quite subtle and will be demonstrated in the following.

Detailed analysis[14] shows that in a relativistic framework the contact density ρ_0 has contributions from atomic $s_{1/2}$ and $p_{1/2}$ orbitals only, from the large and small components, respectively. These contributions are compiled in Table 6 for the neutral iron atom. The table also illustrates that the contact density as expected overestimates the effective density $\bar{\rho}_e$, yet for the iron atom constitutes a good approximation to it, since the error is on the order of merely 1%. Comparison between calculated effective and contact densities for molecules **1–8** furthermore shows that this 1% error is quite systematic in nature (see Tables S5–S7 in the ESI†). On the other hand, the effective density can be calculated at the same computational cost and is therefore recommended.

We have tried to rationalize the variations in isomer shifts of the model structures for [Fe]-hydrogenase by means of projection analysis.[63,64] The projection analysis is based on the expansion of molecular orbitals $\{\psi_k^{\mathrm{MO}}\}$ into a set of pre-calculated atomic orbitals $\{\psi_i^{\mathrm{A}}\}$

$$\psi_k^{\mathrm{MO}} = \sum_{\mathrm{A}} \sum_{i \in \mathrm{A}} \psi_i^{\mathrm{A}} c_{ik}^{\mathrm{A}} + \psi_k^{\mathrm{pol}} \qquad (10)$$

where the orthogonal complement ψ_k^{pol} is denoted the polarization contribution and should in general be small for a meaningful analysis. Insertion of eqn (10) into the SCF expression the expectation value of an operator $\hat{\Omega} = \sum_k^{\mathrm{occ}} \left\langle \psi_k \middle| \hat{\Omega} \middle| \psi_k \right\rangle$ at the SCF-level gives

$$\langle \Omega \rangle = \sum_{\mathrm{A}} \sum_{i \in \mathrm{A}} \sum_{\mathrm{B}} \sum_{j \in \mathrm{B}} \left\langle \psi_i^{\mathrm{A}} \middle| \hat{\Omega} \middle| \psi_j^{\mathrm{B}} \right\rangle D_{ji}^{\mathrm{BA}} + \langle \mathrm{pol} \rangle, \qquad (11)$$

where $D_{ji}^{\mathrm{BA}} = \sum_k^{\mathrm{occ}} c_{ik}^{\mathrm{A}*} c_{jk}^{\mathrm{B}}$ is the density matrix in the fragment basis. In the above expression one may distinguish *intra-atomic* (A = B) and *inter-atomic* (A ≠ B) contributions. Setting the above operator $\hat{\Omega} = 1$ we can carry out a population analysis similar to the Mulliken one, but without the strong basis set dependence.[63]

In Table 7 we give the electron configuration and charge of iron in molecules **6–8** obtained from gross populations. The calculated charges Q of iron in molecules **7** and **8** are indeed quite similar, but somewhat larger than the Mulliken charges reported by Yang and Hall,[42] and consistent with a Fe^{II} rather than a Fe^0 oxidation state. As already stated above, the charges do not correlate well with the calculated isomer shifts reported in Table 5. We also note that the 3d populations of **7** and **8** are basically identical, and so the difference in isomer shifts cannot be attributed to a screening mechanism whereby increased 3d population implies increased screening and thereby reduced contact density of the 3s orbitals in particular.[8,18]

We therefore turn to projection analysis, summarized in Table 8, which shows that the Fe contact density for all three species is, as expected, dominated by intra-atomic contributions from the iron center itself. The intra-atomic contributions further split into diagonal ($j = i$) and hybridization ($j \neq i$) contributions, *cf.* eqn (11), where the latter contributions arise from the breakdown of atomic symmetry in the molecule. Hybridization contributions involving the same atomic types, *e.g.* $s_{1/2}$, may also be associated with a radial re-polarization of atomic orbitals within the molecule. From Table 8 it is seen that the hybridization contributions to **7** and **8** are quite similar and distinct from those of **6**. The major difference between molecules **7** and **8** originates from the diagonal contribution involving the Fe $3s_{1/2}$ orbitals. The value of the diagonal density matrix element $D_{3s,3s}^{\mathrm{Fe,Fe}}$ is 2.1175, 2.1094 and 2.1156 for molecules **6**, **7** and **8**, respectively, compared to rigorously 2.0000 for the neutral iron atom. The differences are very small, but become crucial when multiplied with the atomic matrix element (92.03 a_0^{-3}) in eqn (11). Values larger than two of the diagonal density matrix element arises from overlap of the iron $3s_{1/2}$ orbital with ligand orbitals. In molecule **8** we find for instance overlap on the order of 0.13 between 3s and the hydride coordinated to iron. In summary, our analysis shows that the small, but significant difference in isomer shifts between molecules **7** and **8** arises as the result of overlap between iron core orbitals and ligand orbitals. Such an overlap effect has been discussed previously,[80–83] but in the

Table 6 Orbital contributions (in a_0^{-3}) to the contact density ρ_0 and effective density $\bar{\rho}_e$ of the iron atom in its ground state electron configuration [Ar]$3d^6 4s^2$ obtained with the PBE0 functional and the X2C Hamiltonian. Negligible contributions to $\bar{\rho}_e$ from the $np_{3/2}$, $3d_{3/2}$ and $3d_{5/2}$ orbitals have been omitted from the table

Orbital	ρ_0	$\bar{\rho}_e$
$1s_{1/2}$	13642.75	13463.36
$2s_{1/2}$	1283.89	1266.99
$3s_{1/2}$	184.07	181.64
$4s_{1/2}$	11.16	11.01
$2p_{1/2}$	6.16	6.16
$2p_{1/2}$	0.85	0.85
Total	15128.87	14930.02

Table 7 Electron configuration and charge of iron in molecules **6–8** from projection analysis

	3d	4s	4p	Q^{Fe}
6	6.74	0.20	0.21	+0.86
7	6.79	0.26	0.24	+0.70
8	6.77	0.27	0.27	+0.69

Table 8 Projection analysis of Fe contact density (in a_0^{-3}), relative to the ground state atom, at the X2C/PBE0 level

		6	**7**	**8**
Fe (intra)		−4.15	−4.08	−3.54
pm ($i = j$)		4.02	3.20	3.83
	$1s_{1/2}$	0.59	0.55	0.58
	$2s_{1/2}$	2.98	2.75	2.90
	$2p_{1/2}$	0.00	0.00	0.00
	$3s_{1/2}$	10.81	10.07	10.64
	$3p_{1/2}$	0.01	0.01	0.02
	$4s_{1/2}$	−10.39	−10.18	−10.30
hyb ($i \neq j$)		−8.17	−7.29	−7.36
Interatomic contribution		−0.37	−0.35	−0.38
Polarization contribution		−0.68	−0.71	−0.75
Total		−5.18	−5.15	−4.66

context of molecular wave functions assembled from pre-calculated atomic orbitals and where iron orbitals where projected out from ligand ones for orthonormality. This can be contrasted with the present approach in which fully relaxed molecular orbitals are expanded in pre-calculated atomic ones. Before concluding, it should be noted that a non-relativistic fitting scheme captures the overlap effect as well: using the non-relativistic PBE0 values from Table 2 we obtain isomer shifts 0.050, 0.040 and -0.100 mm s^{-1} for molecules **6**, **7** and **8**, respectively.

4 Conclusion

We have investigated relativistic Hamiltonians of increasing sophistication for the calculation of isomer shift of iron compounds. The set of chosen Hamiltonians comprises the four-component Dirac–Coulomb as well as the two-component X2C Hamiltonians with or without spin–orbit coupling. In addition, all relativistic data have been compared to results obtained with the conventional non-relativistic Schrödinger Hamiltonian. Similar accuracy is achieved for both the full four-component reference Hamiltonian as well as the X2C Hamiltonian, though the latter is computationally less expensive. Further computational savings are possible since spin–orbit coupling can also safely be neglected. Linear correlation plots using effective densities *versus* experimental isomer shift yield a slope of $a = -0.294\ a_0^3$ mm s^{-1} (PBE functional) which is in close agreement with experimentally derived[27] isomer shift calibration constant $\alpha = -0.31\ a_0^3$ mm s^{-1}. Using this correlation constant isomer shifts of very similar quality can be obtained both with and without fitting. The non-relativistic approach gives a significantly different slope and therefore requires fitting. As such its performance is perfectly reasonable. We would still recommend a relativistic approach since scalar relativistic calculations can be carried out at *identical* cost to non-relativistic ones and is the only approach that allows, combined with experiment, us to pinpoint the calibration constant α and thus possibly extract nuclear parameters. The present work also demonstrates that not only valence orbitals, but also subvalence orbitals such as iron 3s, for which relativistic effects become more important, can contribute decisively to isomer shifts. It is also interesting to note that Gubler *et al.*[43] observed a somewhat larger spread in their non-relativistic calibration compared to their relativistic one, within the restricted range of isomer shifts.

Using either method—with and without fitting—the X2C/DFT model is applied to three forms of [Fe]-hydrogenase, which have been proposed to be involved in its catalytic cycle of H_2 cleavage. For these systems we find that both a form without H_2 (**6**) and the intermediate with H_2 bound side-on to the Fe center (**7**) have similar isomer shifts which are in good agreement with the experimental value. Thus, our theoretical results suggest that a Mössbauer study cannot be used to discriminate between these two states. The third discussed state – the hydride intermediate **8** – has a calculated isomer shift that does not only differ significantly from the experimental shift but also from those of **6** and **7**. These findings prompt the conclusion that **8** does not build up in significant concentrations during the Mössbauer experiment. Projection analysis of the associated contact density of the molecules **6–8** reveals that the difference in isomer shift between intermediates **7** and **8** arises primarily from small, but non-negligible overlap between the iron 3s orbital and ligand orbitals, in particular the 1s orbital of the hydride coordinated to iron in **8**.

In this work our primary focus has been on closed-shell iron complexes. Although we expect that our present conclusions will hold also in the more general case of open-shell/high-spin iron complexes we will discuss these issues in a forthcoming publication using a genuine, relativistic open-shell two- and four-component self-consistent-field approach.

Acknowledgements

SK gratefully acknowledges a postdoctoral research grant from the Natural Science Foundation (FNU) of the Danish Agency for Science, Technology and Innovation (grant number: 10-082944) during his postdoctoral stay at SDU Odense. EDH gratefully acknowledges stipends from the OTICON and Augustines foundations. TS would like to acknowledge helpful discussions with V. Nemykin (Duluth) and Eckard Bill (Mülheim). The authors thank the Danish Center for Scientific Computing (DCSC) for computational resources.

References

1 J. C. Fontecilla-Camps, A. Volbeda, C. Cavazza and Y. Nicolet, *Chem. Rev.*, 2007, **107**, 4273–4303.
2 W. Lubitz, E. Reijerse and M. van Gastel, *Chem. Rev.*, 2007, **107**, 4331–4365.
3 R. L. Mössbauer, *Z. Phys.*, 1958, **151**, 124–143.
4 P. Gütlich, E. Bill and A. X. Trautwein, *Mössbauer Spectroscopy and Transition Metal Chemistry. Fundamentals and Applications*, Springer, Heidelberg, 2011.
5 P. Gütlich and C. Schröder, *Bunsenmagazin*, 2010, **12**, 4–22.
6 A. C. Melissinos and S. P. Davis, *Phys. Rev.*, 1959, **115**, 130–137.
7 O. C. Kistner and A. W. Sunyar, *Phys. Rev. Lett.*, 1960, **4**, 412–415.
8 L. R. Walker, G. K. Wertheim and V. Jaccarino, *Phys. Rev. Lett.*, 1961, **6**, 98–101.
9 M. Filatov, *J. Chem. Phys.*, 2007, **127**, 084101.
10 M. Filatov, *Coord. Chem. Rev.*, 2009, **253**, 594–605.
11 M. Filatov, W. Zou and D. Cremer, *J. Chem. Theory Comput.*, 2012, **8**, 875–882.
12 M. Filatov, W. Zou and D. Cremer, *Int. J. Quantum Chem.*, 2013, DOI: 10.1002/qua.24578.
13 B. Fricke and J. T. Waber, *Phys. Rev. B: Solid State*, 1972, **5**, 3445.
14 S. Knecht, S. Fux, R. van Meer, L. Visscher, M. Reiher and T. Saue, *Theor. Chem. Acc.*, 2011, **129**, 631–650.
15 K. J. Duff, *Phys. Rev. B: Solid State*, 1974, **9**, 66–72.
16 A. Trautwein, F. E. Harris, A. J. Freeman and J. P. Desclaux, *Phys. Rev. B: Solid State*, 1975, 4101–4105.

17 W. C. Nieuwpoort, D. Post and P. T. van Duijnen, *Phys. Rev. B: Solid State*, 1978, **17**, 91–98.
18 F. Neese, *Inorg. Chim. Acta*, 2002, **337**, 181–192.
19 A. Reschke, A. Trautwein and J. P. Desclaux, *J. Phys. Chem. Solids*, 1977, **38**, 837–841.
20 Y. Zhang, J. Mao and E. Oldfield, *J. Am. Chem. Soc.*, 2002, **124**, 7829–7839.
21 M. Li, D. Bonnet, E. Bill, F. Neese, T. Weyhermüller, N. Blum, D. Sellmann and K. Wieghardt, *Inorg. Chem.*, 2002, **41**, 3444–3456.
22 Y. Zhang and E. Oldfield, *J. Am. Chem. Soc.*, 2004, **126**, 4470–4471.
23 A. D. Bochevarov, R. A. Friesner and S. J. Lippard, *J. Chem. Theory Comput.*, 2010, **6**, 3735–3749.
24 R. Kurian and M. Filatov, *J. Chem. Theory Comput.*, 2008, **4**, 278–285.
25 R. Kurian and M. Filatov, *Phys. Chem. Chem. Phys.*, 2010, **12**, 2758–2762.
26 U. D. Wdowik and K. Ruebenbauer, *Phys. Rev. B: Condens. Matter Mater. Phys.*, 2007, **76**, 155118.
27 J. Ladrière, A. Meykens, R. Coussement, M. Cogneau, M. Boge, P. Auric, R. Bouchez, A. Banabed and J. Godard, *J. Phys. Colloid Chem.*, 1979, **40**, 20–22.
28 S. J. Rothman, N. L. Peterson, W. K. Chen, J. J. Hines, R. Bastar, L. C. Robinson, L. J. Nowicki and J. B. Anderson, *Phys. Rev. C: Nucl. Phys.*, 1974, **9**, 2272–2274.
29 J. V. Mallow, A. J. Freeman and J. P. Desclaux, *Phys. Rev. B: Solid State*, 1976, **13**, 1884–1892.
30 W. Bambynek, H. Behrens, M. H. Chen, B. Crasemann, M. L. Fitzpatrick, K. W. D. Ledingham, H. Genz, M. Mutterer and R. L. Intemann, *Rev. Mod. Phys.*, 1977, **49**, 77–221.
31 O. Visser, L. Visscher, P. J. C. Aerts and W. C. Nieuwpoort, *Theor. Chem. Acc.*, 1992, **81**, 405–416.
32 T. Saue, *ChemPhysChem*, 2011, **12**, 3077–3094.
33 E. van Lenthe, E. J. Baerends and J. G. Snijders, *J. Chem. Phys.*, 1993, **99**, 4597–4610.
34 C. Chang, M. Pelissier and P. Durand, *Phys. Scr.*, 1986, **34**, 394–404.
35 R. Kurian and M. Filatov, *J. Chem. Phys.*, 2009, **130**, 124121.
36 K. G. Dyall, *J. Chem. Phys.*, 1997, **106**, 9618–9626.
37 M. Iliaš and T. Saue, *J. Chem. Phys.*, 2007, **126**, 064102.
38 T. Hiromoto, K. Ataka, O. Pilak, S. Vogt, M. S. Stagni, W. Meyer-Klaucke, E. Warkentin, R. K. Thauer, S. Shima and U. Ermler, *FEBS Lett.*, 2009, **583**, 585–590.
39 S. Shima, S. Pilak, O. abnd Vogt, M. Schick, M. S. Stagni, W. Meyer-Klaucke, E. Warkentin, R. K. Thauer and U. Ermler, *Science*, 2008, **321**, 572–575.
40 S. Shima and U. Ermler, *Eur. J. Inorg. Chem.*, 2011, 963–972.
41 S. Shima, E. J. Lyon, R. K. Thauer, B. Mienert and E. Bill, *J. Am. Chem. Soc.*, 2005, **127**, 10430–10435.
42 X. Yang and M. B. Hall, *J. Am. Chem. Soc.*, 2009, **131**, 10901–10908.
43 J. Gubler, A. R. Finkelmann and M. Reiher, *Inorg. Chem.*, 2013, **52**, 14205–14215.
44 M. J. Frisch, G. W. Trucks, H. B. Schlegel, G. E. Scuseria, M. A. Robb, J. R. Cheeseman, G. Scalmani, V. Barone, B. Mennucci, G. A. Petersson, H. Nakatsuji, M. Caricato, X. Li, H. P. Hratchian, A. F. Izmaylov, J. Bloino, G. Zheng, J. L. Sonnenberg, M. Hada, M. Ehara, K. Toyota, R. Fukuda, J. Hasegawa, M. Ishida, T. Nakajima, Y. Honda, O. Kitao, H. Nakai, T. Vreven, J. A. Montgomery Jr., J. E. Peralta, F. Ogliaro, M. Bearpark, J. J. Heyd, E. Brothers, K. N. Kudin, V. N. Staroverov, R. Kobayashi, J. Normand, K. Raghavachari, A. Rendell, J. C. Burant, S. S. Iyengar, J. Tomasi, M. Cossi, N. Rega, J. M. Millam, M. Klene, J. E. Knox, J. B. Cross, V. Bakken, C. Adamo, J. Jaramillo, R. Gomperts, R. E. Stratmann, O. Yazyev, A. J. Austin, R. Cammi, C. Pomelli, J. W. Ochterski, R. L. Martin, K. Morokuma, V. G. Zakrzewski, G. A. Voth, P. Salvador, J. J. Dannenberg, S. Dapprich, A. D. Daniels, Ö. Farkas, J. B. Foresman, J. V. Ortiz, J. Cioslowski and D. J. Fox, *Gaussian 09 Revision A.1*, 2009, Gaussian Inc., Wallingford, CT, 2009.
45 A. D. Becke, *Phys. Rev. A*, 1988, **38**, 3098.
46 J. P. Perdew, *Phys. Rev. B: Condens. Matter Mater. Phys.*, 1986, **33**, 8822.
47 A. Schäfer, H. Horn and R. Ahlrichs, *J. Chem. Phys.*, 1992, **97**, 2571.
48 A. Schäfer, C. Huber and R. Ahlrichs, *J. Chem. Phys.*, 1994, **100**, 5829.
49 U. Ryde and M. H. M. Olsson, *Int. J. Quantum Chem.*, 2001, **81**, 335–347.
50 U. Ryde, L. Olsen and K. Nilson, *J. Comput. Chem.*, 2002, **23**, 1058–1070.
51 DIRAC, a relativistic ab initio electronic structure program, Release DIRAC12 (2012), written by H. J. Aa. Jensen, R. Bast, T. Saue, L. Visscher, with contributions from V. Bakken, K. G. Dyall, S. Dubillard, U. Ekström, E. Eliav, T. Enevoldsen, T. Fleig, O. Fossgaard, A. S. P. Gomes, T. Helgaker, J. K. Lærdahl, Y. S. Lee, J. Henriksson, M. Iliaš, Ch. R. Jacob, S. Knecht, S. Komorovský, O. Kullie, C. V. Larsen, H. S. Nataraj, P. Norman, G. Olejniczak, J. Olsen, Y. C. Park, J. K. Pedersen, M. Pernpointner, K. Ruud, P. Sałek, B. Schimmelpfennig, J. Sikkema, A. J. Thorvaldsen, J. Thyssen, J. van Stralen, S. Villaume, O. Visser, T. Winther and S. Yamamoto (see http://www.diracprogram.org).
52 B. A. Hess, C. M. Marian, U. Wahlgren and O. Gropen, *Chem. Phys. Lett.*, 1996, **251**, 365–371.
53 B. Schimmelpfennig, *AMFI: An Atomic Mean-Field Code*, Stockholm, Sweden, 1996.
54 S. H. Vosko, L. Wilk and M. Nusair, *Can. J. Phys.*, 1980, **58**, 1200–1211.
55 J. P. Perdew, K. Burke and M. Ernzerhof, *Phys. Rev. Lett.*, 1996, **77**, 3865–3868.
56 J. P. Perdew, M. Ernzerhof and K. Burke, *J. Chem. Phys.*, 1996, **105**, 9982–9985.
57 T. H. Dunning Jr., *J. Chem. Phys.*, 1989, **90**, 1007–1023.
58 K. G. Dyall, private communication, 2012.
59 Comparison between ρ_0^{HF} with and without contracted ligand basis functions showed that contracted basis sets on the surrounding ligand atoms has only negligible influence on the isomer shifts of the central iron atom.
60 L. Visscher, T. J. Lee and K. G. Dyall, *J. Chem. Phys.*, 1996, **105**, 8769–8776.

61 L. Visscher, E. Eliav and U. Kaldor, *J. Chem. Phys.*, 2001, **115**, 9720–9726.
62 M. Pernpointner and L. Visscher, *J. Comput. Chem.*, 2003, **24**, 754–759.
63 S. Dubillard, J.-B. Rota, T. Saue and K. Fægri, *J. Chem. Phys.*, 2007, **124**, 154307.
64 R. Bast, A. Koers, A. S. P. Gomes, M. Iliaš, L. Visscher, P. Schwerdtfeger and T. Saue, *Phys. Chem. Chem. Phys.*, 2010, **13**, 854.
65 M. Radoń and K. Pierloot, *J. Phys. Chem. A*, 2008, **112**, 11824–11832.
66 M. Radoń, E. Broclawik and K. Pierloot, *J. Phys. Chem. B*, 2010, **114**, 1518–1528.
67 K. Boguslawski, C. R. Jacob and M. Reiher, *J. Chem. Theory Comput.*, 2011, **7**, 2740–2752.
68 P. Schwerdtfeger, T. Söhnel, M. Pernpointer, J. K. Laerdahl and F. E. Wagner, *J. Chem. Phys.*, 2001, **115**, 5913–5923.
69 H. S. Nataraj, M. Kállay and L. Visscher, *J. Chem. Phys.*, 2010, **133**, 234109.
70 M. Kállay and P. R. Surján, *J. Chem. Phys.*, 2001, **115**, 2945.
71 MRCC, a string-based quantum chemical program suite written by M. Kállay. See also ref. 70 as well as http://www.mrcc.hu/.
72 V. N. Nemykin and R. G. Hadt, *Inorg. Chem.*, 2006, **45**, 8297–8307.
73 W. Kerler, W. Neuwirth and E. Fluck, *Z. Phys.*, 1963, **175**, 200–220.
74 W. Kerler and W. Neuwirth, *Z. Phys.*, 1962, **167**, 176–193.
75 R. Greatrex and N. N. Greenwood, *Discuss. Faraday Soc.*, 1969, **47**, 126–135.
76 P. Kuhn, U. Hauser and W. Neuwirth, *Z. Phys.*, 1973, **264**, 287–300.
77 M. A. De Paoli, S. M. de Oliveira, E. Baggio-Saitovitch and D. Guenzburger, *J. Chem. Phys.*, 1984, **80**, 730–734.
78 A. R. Finkelmann, M. T. Stiebritz and M. Reiher, *J. Phys. Chem. B*, 2013, **117**, 4806–4817.
79 H. Tamura, M. Salomone-Stagni, T. Fujishiro, E. Warkentin, W. Meyer-Klaucke, U. Ermler and S. Shima, *Angew. Chem., Int. Ed.*, 2013, **52**, 9656–9659, DOI: 10.1002/anie.201305089.
80 W. H. Flygare and D. W. Hafemeister, *J. Chem. Phys.*, 1965, **43**, 789–794.
81 E. Šimánek and Z. Šroubek, *Phys. Rev.*, 1967, **163**, 275–279.
82 P. F. Walch and D. E. Ellis, *Phys. Rev. B: Solid State*, 1973, **7**, 903–907.
83 A. Trautwein and F. E. Harris, *Theor. Chim. Acta*, 1973, **30**, 45–58.